

12

# A GENERALIZED SIDELobe CANCELLING STRUCTURE FOR ADAPTIVE ARRAYS

AD A 074899

By: L. J. GRIFFITHS      C. W. JIM  
Signal Processing Laboratory  
Department of Electrical Engineering  
University of Colorado

LEVEL <sup>A</sup>

Prepared for:

ELECTRONIC SYSTEMS DIVISION (AFSC)  
OVER-THE-HORIZON RADAR SPO  
HANSCOM AFB, MASSACHUSETTS 01731

CONTRACT N00014-75-C-0830  
(NR 088-076)

through

SRI International  
333 Ravenswood Avenue  
Menlo Park, California 94025  
(415) 326-6200  
Cable: SRI INTL MNP  
Twx: 910-373-1246

10  
251

DDC FILE COPY

Approved for public release; distribution unlimited.

DDC  
RECEIVED  
OCT 10 1979  
A

10 00 002

The views and conclusions contained in this document are those of the authors and should not be interpreted as necessarily representing the official policies, either expressed or implied, of the U.S. Air Force or the U.S. Government.

Technical Report SPL 78-2

11 November 1978

125

# A GENERALIZED SIDELobe CANCELLING STRUCTURE FOR ADAPTIVE ARRAYS.

By: L. J. GRIFFITHS    C. W. JIM  
Signal Processing Laboratory  
Department of Electrical Engineering  
University of Colorado

Prepared for:

ELECTRONIC SYSTEMS DIVISION (AFSC)  
OVER-THE-HORIZON RADAR SPO  
HANSCOM AFB, MASSACHUSETTS 01731

SRI International Subcontract 14107  
under 15  
CONTRACT N00014-75-C-0930  
(NR 088-076)

through

SRI International  
333 Ravenswood Avenue  
Menlo Park, California 94025

Approved for public release; distribution unlimited.

This research was sponsored by the Electronic Systems Division, Air Force Systems Command, through an SRI International subcontract, and was monitored by the Office of Naval Research under Contract No. N00014-75-C-0930 (NR 088-076).

Approved by:

L. J. GRIFFITHS, Project Director  
University of Colorado

|                    |                                     |
|--------------------|-------------------------------------|
| Accession For      |                                     |
| NTIS GRA&I         | <input checked="" type="checkbox"/> |
| DDC TAB            | <input type="checkbox"/>            |
| Unannounced        | <input type="checkbox"/>            |
| Justification      |                                     |
| By _____           |                                     |
| Distribution/      |                                     |
| Availability Codes |                                     |
| Dist.              | Avail and/or special                |
| A                  |                                     |



UNCLASSIFIED

SECURITY CLASSIFICATION OF THIS PAGE (When Data Entered)

19. KEY WORDS (Continued)

20 ABSTRACT (Continued)

approaches in which the constraints have been incorporated into the adaptive algorithm. Another advantage of the GSC formulation is that it clearly delineates the similarities and differences between P-vector and linearly constrained adaptive beamforming.

To assess further the performance characteristics of adaptive processing of HF radar data, the GSC beamformer was used to study data collected at the Wide Aperture Research Facility operated by SRI International. Findings of this study are included.

UNCLASSIFIED

SECURITY CLASSIFICATION OF THIS PAGE (When Data Entered)

## CONTENTS

|   | <u>Page</u> |
|---|-------------|
| I. INTRODUCTION                                     | 1           |
| II. THE GENERALIZED SIDELOBE CANCELLING ARRAY MODEL | 3           |
| <u>Preliminaries</u>                                | 3           |
| <u>Generalized Sidelobe Cancelling</u>              | 5           |
| <u>P-Vector and Linear Constraint Beamforming</u>   | 9           |
| <u>Extensions to Other Beamforming Processors</u>   | 12          |
| <u>Summary</u>                                      | 17          |
| III. EXPERIMENTAL RESULTS                           | 19          |
| i) <u>Convergence Time Constant Studies</u>         | 23          |
| a) <u>Increased Adaptive Step Size</u>              | 25          |
| b) <u>Conjugate Gradient Adaptation</u>             | 27          |
| ii) <u>Array Element Gain Variation Studies</u>     | 33          |
| iii) <u>Optimum Choice of Initial Weight Vector</u> | 37          |
| IV. DISCUSSION AND CONCLUSIONS                      | 42          |
| References  | 44          |

## TABLES

|   |    |
|---|----|
| Table I: Signal, interference, and spurious parameters for conjugate gradient algorithm ( $\alpha = 0.16$ , 4 taps/element, $W_S = D$ ) | 28 |
| Table II: Signal, interference, and spurious parameters for doppler spectra shown in Figs. 7-13   | 33 |

## ILLUSTRATIONS

|   | <u>Page</u> |
|---|-------------|
| Fig. 1: Generalized adaptive beamformer used in previous WARF data studies.   | 6           |
| Fig. 2: Basic form of generalized sidelobe cancelling adaptive array structure.                                       | 7           |
| Fig. 3: Beampattern for uniform-weighted conventional array processor. (Normalized to grating lobe spacing)           | 20          |
| Fig. 4: Beampatterns for Walsh function preprocessor  |             |
| a) Walsh #1 + + + + - - - -   | 21          |
| b) Walsh #2 + + - - - - + +   | 21          |
| c) Walsh #3 + - - + + - - +   | 21          |
| d) Walsh #4 + + - - + + - -   | 21          |
| e) Walsh #5 + - - + - + + -   | 22          |
| f) Walsh #6 + - + - - + - +   | 22          |
| g) Walsh #7 + - + - + - + -   | 22          |
| Fig. 5: Beampattern for difference preprocessor   | 22          |
| Fig. 6: Range-doppler map for 1-sec dwell from WARF tape RML 0030, File No. 64, using conventional beamformer.        | 24          |
| Fig. 7: Doppler spectrum using conventional beamformer.   | 24          |
| Fig. 8: Doppler spectrum using 1st order adaptive algorithm with no pre-adaptation, $\alpha = 0.16$ .                 | 29          |
| Fig. 9: Doppler spectrum using 2nd order adaptive algorithm with no pre-adaptation, $\alpha = 0.16$ , $\beta = 0.5$ . | 29          |
| Fig. 10: Doppler spectrum using 1st order adaptive algorithm with pre-adaptation, $\alpha = 0.16$ .                   | 31          |

|  | <u>Page</u> |
|--|-------------|
| Fig. 11: Doppler spectrum using 2nd order adaptive algorithm<br>with pre-adaptation, $\alpha = 0.16$ , $\beta = 0.5$ .             | 31          |
| Fig. 12: Doppler spectrum using 1st order adaptive algorithm<br>only during pre-adaptation period, $\alpha = 0.16$ .               | 32          |
| Fig. 13: Doppler Spectrum using 2nd order adaptive algorithm<br>only during pre-adaptation period, $\alpha = 0.16$ , $\beta = 0.5$ | 32          |
| Fig. 14: Signal-to-interference ratios observed as a function<br>of array geometry using difference preprocessor.                  | 36          |
| Fig. 15: Doppler spectra with elements 1,3,4 set to zero   |             |
| a) Conventional beamforming  | 38          |
| b) Linearly constrained adaptive beamforming   | 38          |
| c) P-vector adaptive beamforming   | 39          |
| Fig. 16: Signal-to-interference ratios observed as a function<br>of array geometry using Walsh preprocessor.                       | 40          |

## 1 INTRODUCTION

Previous reports prepared by the University of Colorado on the topic of adaptive array processing [1-5] have described the application of well-known adaptive methods to over-the-horizon (OTH) radar data. Two specific implementations have been studied: P-vector adaptation and Frost's linearly constrained structure. This work has shown that both methods provide increased output SNR compared with a conventionally weighted beamformer. In addition, significant differences between the two methods were noted, particularly with respect to convergence rate, the effect of MTI preprocessing, and final SNR improvement.

The purpose of the present report is to provide a description of an overall optimal beamformer structure designed to operate in a specific radar format. It is assumed that the processor must operate during a dwell time of  $T$  seconds (typically,  $T=1$  sec or 64 transmit sweeps) and that the radar is switched to a new frequency and/or azimuth at the beginning of the dwell. In this environment, the adaptive beamformer cannot use data immediately prior to the dwell of interest to allow initial conditions to decay. Rather, these initial transients must take place during the current dwell as data are being collected for range/doppler processing at the beamformed output. It is therefore imperative that the deleterious effects of adaptation transients at the output be minimized.

We present below a summary of a study designed to determine the parameters of an adaptive beamformer designed to minimize these effects. Three interrelated characteristics of the processor are considered in detail:

- i) time constant of convergence
- ii) the effect of gain variations in the array elements
- iii) the effect of initial choice of the weight vector.

Our approach is to examine the response of a given array configurations to each characteristic and to select that having the best overall performance, as determined at the beamformed output.

The results presented below are based on the use of a new formulation for adaptive arrays [6-7]. This formulation allows direct comparison of P-vector and linearly constrained adaptation by showing that these beamformers are both members of a general class termed here Generalized Sidelobe Cancelling Arrays. In addition, a large number of alternative configurations, not previously identified, which also fall into this class are discussed. The new formulation is used to present a theoretical discussion of the adaptive array response to each of the three characteristics listed above. We also describe the results of beamforming experiments which utilize experimental WARF\* data. These latter results are shown to be consistent with the generalized model.

---

\*WARF: Wide Aperture Research Facility. WARF is an HF radar research facility operated by SRI International under primary sponsorship of the Electronic Systems Division of the Air Force Systems Command and the Office of Naval Research.

## II THE GENERALIZED SIDELobe CANCELLING ARRAY MODEL

### Preliminaries

As in previous studies, we assume an array consisting of  $K$  elements which has been time-delay steered to a desired look direction. With  $x_i(k)$  used to denote the  $k^{\text{th}}$  sample of the demodulated output of array element  $i$ , the vector of received samples  $\underline{x}(k)$  is given by

$$\underline{x}(k) = \underline{s}(k) + \underline{n}(k). \quad (1)$$

The vector  $\underline{s}(k)$  is due to the presence of a desired "target" signal and  $\underline{n}(k)$  represents the cumulative effects of all noise and interference terms.

Ideally, with perfect presteering, the desired signal component is identical at all outputs and

$$\underline{s}(k) = d(k)\underline{1} \quad (2)$$

with:  $d(k)$  = scalar desired waveform

$$\underline{1}^T = [1, 1, \dots, 1]$$

In order to model the more realistic case of uncorrected gain variations, we modify Eq. (2) as follows:

$$\underline{s}(k) = d(k)\underline{v} \quad (3)$$

The gain vector  $\underline{v}$  consists of  $K$  channel gains  $v_i$  which represent the individual array element gain values.

In adaptive array processing, a beamformed output  $y_0(k)$  is formed as the sum of delayed and weighted values of the vector of received signals. The weighting coefficients are time-varying in a manner determined by the particular algorithm in use. Thus,

$$y_0(k) = \sum_{\ell=0}^{L-1} w_{\ell}^T(k) \underline{x}(k-\ell) \quad (4)$$

where  $\underline{w}_\ell(k)$  is the set of K coefficients which weight the received signals after a delay of  $\ell$  samples. Equation (4) may also be expressed in a more compact form as

$$y_0(k) = \underline{w}_\ell^T(k) \underline{x}(k) \quad (4a)$$

$$\underline{w}_\ell^T(k) = [\underline{w}_{-0}^T(k), \underline{w}_{-1}^T(k), \dots, \underline{w}_{-L-1}^T(k)] \quad (4b)$$

$$\underline{x}^T(k) = [\underline{x}^T(k), \underline{x}^T(k-1), \dots, \underline{x}^T(k-L-1)] \quad (4c)$$

The adaptive algorithm used to update the adaptive coefficients  $\underline{w}_\ell(k)$  may be expressed in general terms as

$$\underline{w}_\ell(k+1) = \underline{w}_\ell(k) + \underline{\Delta}_\ell(k) \quad (5)$$

The update term  $\underline{\Delta}_\ell(k)$  depends upon the specific algorithm employed. For P-vector adaptation,

$$\underline{\Delta}_\ell^P(k) = \mu [r_d(\ell) \underline{1} - y_0(k) \underline{x}(k-\ell)] \quad (6)$$

where  $r_d(\ell) = E[d(k)d(k-\ell)]$  is the assumed correlation function for the desired signal and  $\mu$  is a scalar constant which determines convergence properties of the algorithm.

When Frost's algorithm for linearly-constrained adaptation is used, the appropriate expression for  $\underline{\Delta}_\ell(k)$  is given by

$$\begin{aligned} \underline{\Delta}_\ell^F(k) = & \mu y_0(k) \underline{x}(k-\ell) + \frac{1}{K} f(\ell) \\ & - \frac{1}{K} \left[ \underline{1}^T \underline{w}_\ell(k) + \mu y_0(k) \underline{1}^T \underline{x}(k-\ell) \right] \underline{1} \end{aligned} \quad (7)$$

The scalar term  $f(\ell)$  is determined by the constraint equations,

$$\underline{1}^T \underline{w}_\ell(k) = f(\ell) \quad (8)$$

and ensures that the frequency response of the array processor in the desired look direction is that of a tapped-delay-line filter with coefficients

$f(0), f(1), \dots, f(L-1)$ . In previous WARF studies, values  $f(l)=0$  except for  $f(L/2)=1$  have been employed, thus ensuring a flat response.

### Generalized Sidelobe Cancelling

Equations (1) through (8) above summarize the adaptive array configurations previously studied--i.e., P-vector adaptation and linearly constrained adaptation. Either of these procedures can be represented by the generalized adaptive beamformer shown in Fig. 1. We now proceed to introduce a general form for an adaptive beamformer and then show that this generalized structure contains both P-vector and linearly constrained methods as special cases.

Figure 2 shows the basic form of the proposed generalized sidelobe cancelling adaptive array structure. The upper, or conventional array, path consists of a set of fixed amplitude taper coefficients  $\underline{w}_c$  which are used to produce a conventionally beamformed output  $y_c(k)$ ,

$$y_c(k) = \underline{w}_c^T \underline{x}(k) \quad (9)$$

For convenience of later notation, we assume that the coefficients in  $\underline{w}_c$  have a sum square of unity--i.e.,  $\underline{w}_c^T \underline{w}_c = 1$ . The signal  $y_c(k)$  corresponds to the best non-adaptive beamformer and, in previous WARF studies, was formed using Dolph-taper values. The conventional output is filtered by an L-coefficient adaptive tapped-delay-line filter to produce  $y'_c(k)$ ,

$$y'_c(k) = \sum_{\ell=0}^{L-1} a'_\ell(k) y_c(k-\ell) \quad (10)$$

Since this is a scalar input/output filter,  $y'_c(k)$  is a temporally filtered version of  $y_c(k)$ . The scalar coefficients  $a'_\ell(k)$  are updated using an algorithm A, to be specified later.

The lower path in Fig. 2 is the sidelobe cancelling path. It consists of a preprocessor  $\underline{W}_S$  followed by a multi-channel adaptive combiner denoted

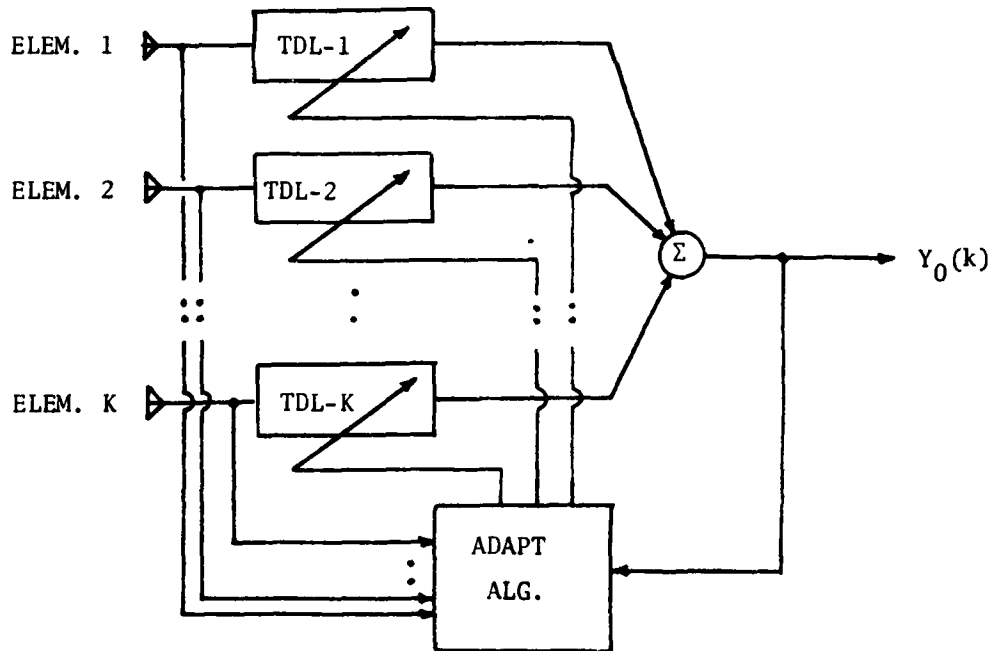


Fig. 1 Generalized adaptive beamformer used in previous WARF data studies.

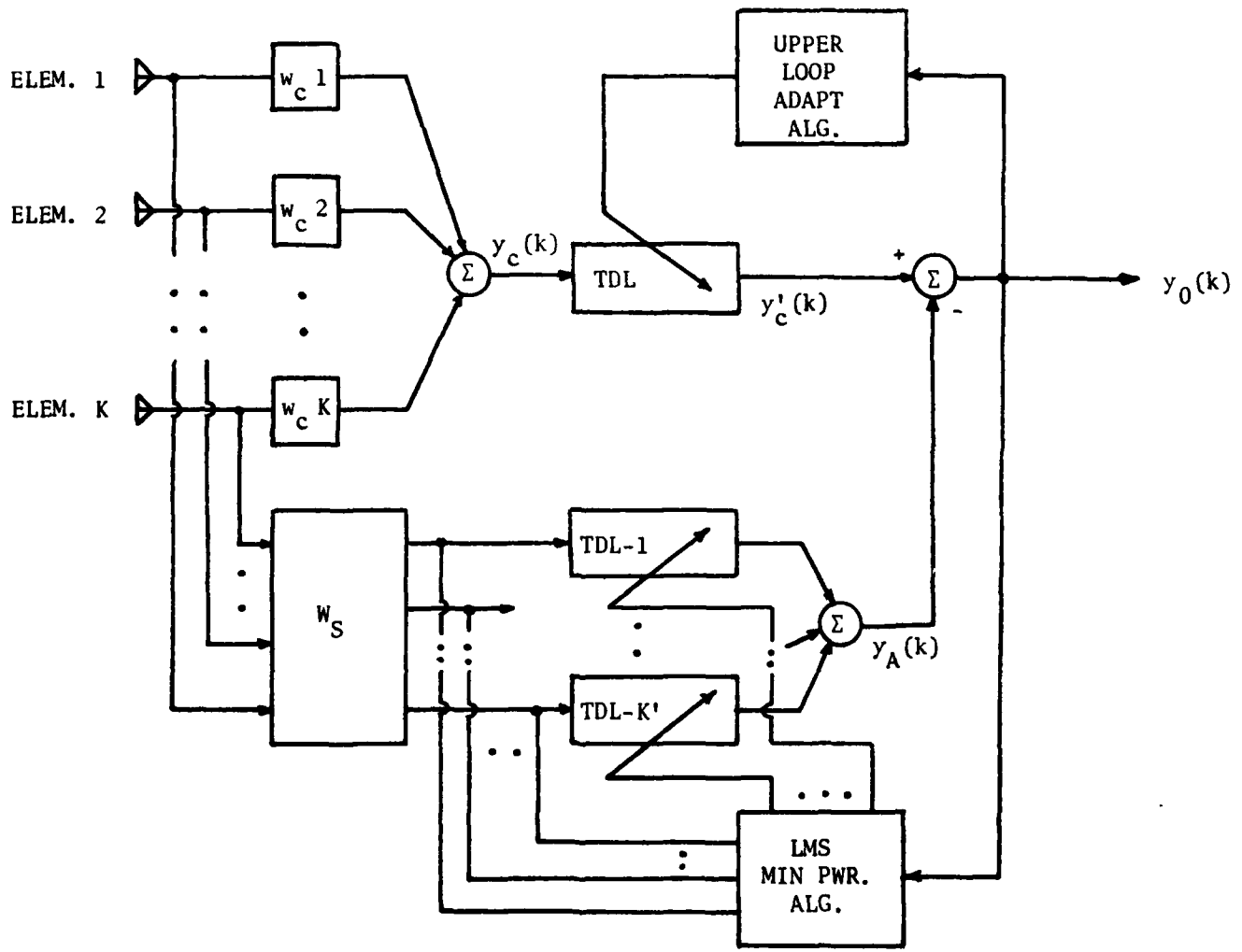


Fig. 2 Basic form of generalized sidelobe cancelling adaptive array structure.

by  $\underline{w}'_{\ell}(k)$ . This combiner consists of a set of tapped-delay-lines, each containing L adaptive coefficients. The scalar output  $y_A(k)$  is the sum of all delayed and weighted terms. The purpose of the lower path is to subtract interference from the modified conventional output  $y'_C(k)$ . This is accomplished by first ensuring that  $\underline{W}_S$  blocks all desired signals from the lower path and secondly by adapting  $\underline{w}'_{\ell}(k)$  to minimize the power in the difference signal  $y_0(k)$ . Minimum power is readily obtained using the LMS algorithm [8].

$$\underline{w}'_{\ell}(k+1) = \underline{w}'_{\ell}(k) + \mu y_0(k) \underline{x}'(k-\ell) \quad (11)$$

where  $\underline{x}'(k)$  is the vector of signals observed at the preprocessor output,

$$\underline{x}'(k) = \underline{W}_S \underline{x}(k) \quad (12)$$

Recall that  $\underline{W}_S$  is required to block the desired signal  $d(k)$ . For the ideally presteered case in Eq.(2), this is accomplished by ensuring that the rows of  $\underline{W}_S$  are orthogonal to the unit vector  $\underline{1}$ . Thus, if  $\underline{b}_i^T$  is the  $i^{\text{th}}$  row of  $\underline{W}_S$ , we require

$$\underline{b}_i^T \underline{1} = 0 \quad , \quad \text{for all } i. \quad (13)$$

Since  $\underline{W}_S$  has K columns (corresponding to the number of array elements), Eq. (13) implies that  $\underline{W}_S$  can have at most K-1 independent rows. Equivalently,  $\underline{x}'(k)$  has at most  $K'=K-1$  elements.

The overall structure shown in Fig. 2 represents the general form of the sidelobe cancelling array structure. Specific forms are obtained by defining the spatial preprocessor  $\underline{W}_S$  matrix and the scalar upper path adaptive algorithm A. As shown below, both P-vector and linearly constrained adaptive processors can be implemented in this manner. The advantages of this configuration are twofold:

- i) In addition to the two specific forms mentioned above, the sidelobe canceller can implement a wide variety of adaptive array structures which exhibit useful practical properties.
- ii) The configuration in Fig. 2 separates out, in a natural manner, both a conventional beamformer and the set of linear constraints. As a result, array adaptation is reduced to its simplest possible form: the unconstrained LMS algorithm.

### P-Vector and Linear Constraint Beamforming

We denote a set of adaptive coefficients used in a P-vector adaptive beamformer by

$$\underline{w}_\ell^P(k) , \ell = 0, 1, \dots, L-1. \quad (14)$$

From Eqs. (5) and (6), the P-vector algorithm is

$$\underline{w}_\ell^P(k+1) = \underline{w}_\ell^P(k) + \mu [r_d(\ell) \underline{1} - y_0(k) \underline{x}(k-\ell)]. \quad (15)$$

where

$$y_0(k) = \sum_{\ell=0}^{L-1} \underline{x}^T(k-\ell) \underline{w}_\ell^P(k). \quad (16)$$

The method used to transform Eqs. (14)-(16) to a sidelobe canceller form involves the use of a  $K \times K$  orthogonal transformation matrix  $\underline{T}$ . The rows of this matrix are orthogonal and normalized to unit length. Thus, if  $\underline{e}_i^T$  represents the  $i^{\text{th}}$  row,

$$\begin{aligned} \underline{e}_i^T \underline{e}_j &= 0 , \quad i \neq j \\ &= 1 \quad i = j \end{aligned}$$

and  $\underline{T}^{-1} = \underline{T}^T$ . Any matrix of this form can be used to rewrite Eq. (16) as

$$y_0(k) = \sum_{\ell=0}^{L-1} \left[ \underline{T} \underline{x}(k-\ell) \right]^T \left[ \underline{T} \underline{w}_\ell^P(k) \right] \quad (17)$$

The appropriate update algorithm for  $\underline{T}w_{\ell}^P(k)$  is then

$$\underline{T}w_{\ell}^P(k+1) = \underline{T}w_{\ell}^P(k) + \mu[r_d(\ell)\underline{T}\underline{1} - y_0(k)\underline{T}x(k-\ell)] \quad (18)$$

We now restrict our attention to  $\underline{T}$  matrices having their first row consist of equal values  $1/\sqrt{K}$ . The matrix is then partitioned as

$$\underline{T} = \begin{bmatrix} \frac{1}{\sqrt{K}} & \underline{1}^T \\ \hline & -\underline{W}_S \end{bmatrix} \quad (19)$$

and, from the discussion above, the rows of  $\underline{W}_S$  are all orthogonal to the unit vector as well as to each other. The reason for the negative sign is that by substituting Eq. (19) in (17) and (18), the processor is directly converted to the sidelobe cancelling form in Fig. 2. The appropriate conventional weights are given by

$$\underline{w}_c = \frac{1}{\sqrt{K}} \underline{1} \quad (20)$$

The algorithm in Eq. (18) may be written as two algorithms, the first corresponding to scalar weights  $a_{\ell}^i(k)$  corresponding to multiplication by the first row of  $\underline{T}$  and a second algorithm for the remaining  $K-1$  weights  $\underline{w}_{\ell}^i(k)$ --i.e.,

$$a_{\ell}^i(k) = \frac{1}{\sqrt{K}} \underline{1}^T w_{\ell}^P(k) \quad (21)$$

$$\underline{w}_{\ell}^i(k) = \underline{W}_S w_{\ell}^P(k) \quad (22)$$

and the appropriate algorithms are:

$$a_{\ell}^i(k+1) = a_{\ell}^i(k) + \mu[K^{-1/2}r_d(\ell) - y_0(k)y_c(k-\ell)] \quad (23)$$

$$\underline{w}'_{\ell}(k+1) = \underline{w}'_{\ell}(k) - \mu y_0(k) \underline{x}'(k-\ell) \quad (24)$$

Equations (23) and (24) are derived by direct substitution of Eqs. (9), (12), (21), and (22) into Eq. (18). The first of these (23) is the algorithm A depicted in Fig. 2 and (24) is the unconstrained LMS algorithm. In summary, the P-vector algorithm used in previous WARF data processing is equivalent to the sidelobe canceller in Fig. 2 with a uniform taper conventional beam ( $\underline{w}_c = \frac{1}{\sqrt{K}} \underline{1}$ ), algorithm A given by (23), and rows of  $\underline{W}_S$  which are mutually orthogonal (as well as orthogonal to  $\underline{1}$ ). One interesting example of a  $\underline{W}_S$  preprocessor with this property occurs when K is a power of 2. The rows of  $\underline{W}_S$  can then be implemented as Walsh functions [9] which consist only of +1 or -1 elements.

Frost's linearly constrained algorithm for a set of adaptive coefficients denoted by  $\underline{w}_{\ell}^F(k)$  is given by (see Eqs. (5) and (7))

$$\begin{aligned} \underline{w}_{\ell}^F(k+1) = & \underline{w}_{\ell}^F(k) + \mu y_0(k) \underline{x}(k-\ell) + \frac{f(\ell)}{K} \underline{1} \\ & - \frac{1}{K} \left[ \underline{1}^T \underline{w}_{\ell}^F(k) + \mu y_0(k) \underline{1}^T \underline{x}(k-\ell) \right] \underline{1}, \end{aligned} \quad (25)$$

where  $y_0(k)$  is computed as in (16) with P replaced by F. Proceeding as above, an orthogonal matrix  $\underline{T}$  is inserted into the expression for  $y_0(k)$  which results in an equation analogous to (17). The update algorithm for  $\underline{T} \underline{w}_{\ell}^F(k)$  is

$$\begin{aligned} \underline{T} \underline{w}_{\ell}^F(k+1) = & \underline{T} \underline{w}_{\ell}^F(k) + \mu y_0(k) \underline{T} \underline{x}(k-\ell) + \frac{f(\ell)}{K} \underline{T} \underline{1} \\ & - \frac{1}{K} \left[ \underline{1}^T \underline{T}^T \underline{T} \underline{w}_{\ell}^F(k) + \mu y_0(k) \underline{1}^T \underline{T}^T \underline{T} \underline{x}(k-\ell) \right] \underline{T} \underline{1} \end{aligned} \quad (26)$$

With  $\underline{T}$  as in (19), this reduces to two subalgorithms: one in a scalar  $a_{\ell}^i(k)$  defined by Eq. (21) and a second in the K-1 dimensional weight vector

$w_{\ell}^i(k)$  defined by (22). These algorithms are:

$$a_{\ell}^i(k+1) = f(\ell)/\sqrt{K} \quad (27)$$

$$w_{\ell}^i(k+1) = w_{\ell}^i(k) - \mu y_0(k) x^i(k-\ell) \quad (28)$$

And, as was the case for P-vector adaptation, Frost's algorithm reduces to the sidelobe canceller form with  $w_c = \frac{1}{\sqrt{K}} \underline{1}$  and  $\underline{W}_S$  containing K-1 orthogonal rows. Note, however, that the algorithm A in this case sets the single-channel tapped-delay-line coefficients equal to fixed, non-adaptive values  $f(\ell)$ --i.e., the constraint values in Eq. (8). In effect, algorithm A is not active and the upper filter is a fixed element in the system. In previous WARF studies, values  $f(\ell)=0$  except for  $f(L/2)=1$  were used and this filter reduced to a simple delay element of L/2 samples. This step is equivalent to  $y_c^i(k) = y_c(-L/2)$  in Fig. 2.

#### Extensions to Other Beamforming Processors

In the discussion presented above, it was shown that both P-vector and linearly constrained adaptive array processors can be implemented as generalized sidelobe cancelling (GSC) arrays. The method used to demonstrate this fact involved inserting an orthogonal matrix  $\underline{T}$ , with the particular structure given by Eq. (19), into the original adaptive algorithms. Rows 2 through K of T in this case must sum to zero, be mutually orthogonal, and orthogonal to the first row.

In this section, we examine generalizations of  $\underline{T}$  which preserve the sidelobe cancelling structure by ensuring that rows 2 through K sum to zero, but we relax the orthogonality constraint. For convenience of notation, we also require that the rows have unit length. Specifically, the form of  $\underline{T}$  is given by

$$\underline{T} = \begin{bmatrix} \underline{e}_1^T \\ \underline{e}_2^T \\ \cdot \\ \underline{e}_K^T \end{bmatrix} = \begin{bmatrix} \underline{w}_c^T \\ \text{---} \\ \underline{-w}_s \end{bmatrix} \quad (29)$$

where

$$\underline{e}_i^T \underline{1} = 0 \quad , \quad i = 2, 3, \dots, K \quad (30)$$

$$\underline{e}_1^T \underline{1} = \underline{w}_c^T \underline{1} = 1 \quad (31)$$

$$\underline{e}_i^T \underline{e}_i = 1 \quad , \quad i = 2, 3, \dots, K \quad (32)$$

and the rows of  $\underline{T}$ ,  $\underline{e}_i^T$ , may or may not be mutually orthogonal.

In general,  $\underline{T}$  matrices constructed in this manner will not be orthogonal, i.e.,  $\underline{T} \underline{T}^T \neq \underline{I}$ . Since the equivalence of the sidelobe cancelling structure was based on orthogonality of  $T$ , the results obtained can therefore no longer be guaranteed to reproduce the original algorithms, and additional analysis must be carried out to determine the properties of the modified processor.

The first row of  $\underline{T}$ ,  $\underline{w}_c^T$ , contains the conventional beamforming weights. For an orthogonal  $\underline{T}$ , this beamformer must have uniform coefficients, as shown by the following. Since  $\underline{T}$  is orthogonal, its rows  $\underline{e}_i^T$  form a basis which can be used to expand the unit vector  $\underline{1}$ ,

$$\underline{1} = \sum_{i=1}^k \beta_i \underline{e}_i \quad (33)$$

where

$$\beta_i = \underline{e}_i^T \underline{1} \quad (34)$$

But, rows 2 through K sum to zero (Eq (30)) and thus  $\beta_i = 0$  for

$i = 2, 3, \dots$ . Using this result, equation (33) may be rewritten as

$$\underline{e}_1 = \frac{1}{\beta_1} \underline{1} \quad (35)$$

and a uniform taper conventional beamformer is mandatory for GSC structures based on an orthogonal transformation.

We now consider the case where  $\underline{w}_c$  is any normalized set of coefficients and the rows of  $\underline{W}_s$  obey Eqs. (30) to (32). In this case, it can be shown that the steady-state adapted weight vectors for both the GSC P-vector algorithm [Eqs. (23) and (24)] and the GSC Frost algorithm (Eqs. (27) and (28)) are equal to the steady-state solutions achieved by the algorithms used in previous studies [Eqs. (5), (6), and (7)]. Thus, one would expect no change in the converged output signal-to-noise ratio or other performance measures based on steady-state performance when a generalized sidelobe cancelling approach to adaptive beamforming. It should be noted, however, that these conclusions require that the  $K-1$  outputs of the spatial preprocessor  $\underline{W}_s$  are linearly independent. Equivalently, the matrix  $\underline{W}_s$  must be full rank with linearly independent rows  $\underline{e}_i$ ,  $i = 2, 3, \dots, K$  in Eqs. (29)-(32).

The equality of the steady-state processors is independent of the type of conventional beamformer  $\underline{w}_c$  which is employed. Any differences which occur as the result of the changes in amplitude shading are compensated for in the lower path of the GSC structure. The method used to demonstrate this independence is identical to that used to derive the equality of the steady-state GSC and previous beamformers. A steady-state weight vector  $\underline{w}_l^M$  is defined as that which causes the next iterated vector  $\underline{w}_l(k+1)$  to equal  $\underline{w}_l^M$  when the expected value of the update algorithm (5) is employed -- i.e.,

$$\underline{w}_l(k+1) = \underline{w}_l^M + E[\Delta_l^M(k)] \quad (36)$$

In this expression,  $\Delta_{\ell}^M(k)$  denotes the fact that  $\underline{w}_{\ell}(k)$  has been replaced by  $\underline{w}_{\ell}^M$  in the update term. Thus, the steady-state weight vector  $\underline{w}_{\ell}^M$  satisfies

$$E[\Delta_{\ell}^M(k)] = 0, \ell = 0, 1, \dots, L-1 \quad (37)$$

and can be determined directly from (6), (7), (18) or (25). It is a simple matter to verify that (6) and (18) lead to the same solution and that (7) and (19) also produce identical results.

In comparing the dynamics of adaptation from an initial starting point  $\underline{w}_{\ell}(0)$  to the steady-state solutions, however, significant differences arise between the GSC methods and previous techniques. It is well known [8,10] that the dynamical behavior of the algorithm is determined by the covariance matrix of the set of signals observed at the individual processor weights. In previous studies, this vector was the vector of array element signals  $\underline{x}(k)$  as shown by (4). The appropriate covariance matrix is then  $\underline{R}_{XX}$  given by

$$\underline{R}_{XX} = E[\underline{x}(k)\underline{x}^T(k)] \quad (38a)$$

$$= \begin{bmatrix} E[\underline{x}(k)\underline{x}^T(k)] & \dots & E[\underline{x}(k)\underline{x}^T(k-L-1)] \\ E[\underline{x}(k-1)\underline{x}^T(k)] & & \\ \cdot & & \\ \cdot & & \\ E[\underline{x}(k-L-1)\underline{x}^T(k)] & \dots & E[\underline{x}(k-L-1)\underline{x}^T(k-L-1)] \end{bmatrix} \quad (38b)$$

which may be partitioned into submatrices  $\underline{R}_{XX}(\ell)$  defined by

$$\underline{R}_{XX}(\ell) = E[\underline{x}(k)\underline{x}^T(k-\ell)] \quad (39)$$

The eigenvalues of  $\underline{R}_{XX}$  in (38) directly determine the rate of convergence and other dynamical behavior of the appropriate algorithm.

In GSC processing, the vector  $\underline{x}(k-l)$  is premultiplied by the matrix  $\underline{T}$  prior to adaptation. The appropriate covariance matrix is then similar in structure to (38) except that the submatrices become

$$\tilde{\underline{R}}_{XX}(\ell) = \underline{T} \underline{R}_{XX}(\ell) \underline{T}^T \quad (40)$$

The eigenvalues of the resulting covariance matrix will be identical to those of (38) if and only if  $\underline{T}$  is an orthogonal matrix. Thus, in general, we can expect the convergence characteristics of the GSC adaptive beamformer to be identical to that for the previous adaptive processors only if the rows of  $\underline{W}_S$  are mutually orthogonal and if a uniform taper conventional beamformer is used. This latter requirement may be dropped for the case of the GSC Frost algorithm, however, due to the fact that the upper path is non-adaptive and that the conventional beamforming system affects only upper path signals. Further discussion of this fact is presented in Reference [11].

A relevant question which arises in this context is whether or not the GSC processor can provide faster convergence times through appropriate choice of  $\underline{W}_S$  and  $\underline{w}_c$ . Clearly, these beamformers represent a larger class of processors in that the previous methods may be created as a subset from the class. It is therefore reasonable to assume that faster convergence may well be achieved using the GSC approach. This is indeed the case as shown by the following discussion. The adaptive time constant is directly proportional to the eigenvalue spread in the covariance matrix [10], with long time constants resulting from large eigenvalue disparity. For those processors in which  $\underline{T}$  is not orthogonal, the GSC covariance matrix  $\tilde{\underline{R}}_{XX}$  analogous to (38) is

$$\tilde{\underline{R}}_{XX} = \tilde{\underline{T}} \underline{R}_{XX} \tilde{\underline{T}}^T \quad (41)$$

where

$$\tilde{\underline{T}} = \begin{bmatrix} \underline{I} & \underline{0} & \cdot & \cdot & \cdot & \underline{0} \\ \underline{0} & \underline{T} & & & & \cdot \\ \cdot & & & & & \\ \underline{0} & \cdot & \cdot & \cdot & & \underline{T} \end{bmatrix} \quad (42)$$

The minimum convergence time achievable is that which results when  $\underline{T}$  is chosen to produce an identity matrix for  $\underline{R}_{XX}$ . Since  $\underline{R}_{XX}$  is a positive definite matrix, this requires

$$\underline{T} = \underline{R}_{XX}^{1/2} \quad (43)$$

Unless  $\underline{R}_{XX}$  has particularly simple structure -- e.g., that resulting from array signals which are spectrally white -- the matrix  $\underline{T}$  which satisfies (43) will not have the block diagonal structure shown in (42). Thus, in most cases, a GSC processor having a diagonal  $\tilde{\underline{R}}_{XX}$  cannot be found. There will exist a transformation  $\underline{T}$ , however, such that  $\tilde{\underline{R}}_{XX}$  has a smaller eigenvalue spread than does  $\underline{R}_{XX}$ . Unfortunately, this transformation cannot be found without first knowing the value of  $\underline{R}_{XX}$ , or equivalently, without having a complete specification of the array noise and interference environment.

### Summary

In this section we have presented a mathematical formulation for a new beamforming structure, termed a generalized sidelobe cancelling beamformer. It has been shown that this beamformer is a generalization of those used in previous adaptive array studies which allows a much wider class of adaptive arrays to be implemented. The GSC separates out, in a natural manner, both the conventional beamformer and a set of linear constraints. In addition, it illustrates, in a simple manner, the differences between P-vector and Frost-algorithm processing. In the section following, we illustrate how this structure can be further applied to study convergence rates, gain variation effects,

and the effect of initial weight vector choice on the overall performance of an adaptive array. These studies are based on the use of digitized experimental data.

### III. EXPERIMENTAL RESULTS

In this section we present experimental results relating to the three adaptive processor characteristics of interest in this report:

- i) convergence time constant studies
- ii) the effect of array element gain variations
- iii) optimum choice of initial weight vector.

These topics are addressed using the generalized sidelobe cancelling processor described in the previous section. In all cases, a uniform taper conventional beamformer was used in the upper path of the processor. Figure 3 shows the resulting spatial pattern for the conventional array. The spatial angle  $\theta$  shown on this figure has been normalized to the grating lobe spacing of the array and the effects of the subarray beam pattern have not been included.

Two types of spatial preprocessor  $\underline{W}_S$  were studied: 1) an orthogonal structure in which the rows of  $\underline{W}_S$  were chosen as Walsh functions and 2) a non-orthogonal structure consisting of rows containing +0.5 and -0.5 in adjacent locations and zeros elsewhere. The latter case corresponds to taking all possible differences of adjacent subarray outputs, a technique which has been used in monopulse arrays. Figure 4 shows the set of 7 pre-filter array beam patterns which result when the Walsh method (W) is used on eight subarray outputs. Note that all patterns are constrained to have a null at the  $\theta = 0^\circ$  position. In the difference preprocessor (D), every subarray pattern has the response shown in Fig. 5.

The data selected for the experimental studies were recorded at WARF on July 10, 1975. Eastward-looking transmissions at a center frequency of 12.13 MHz were employed and the digitized data were recorded on tape RML 0030, file 64. Two transponders were active during the test, located in

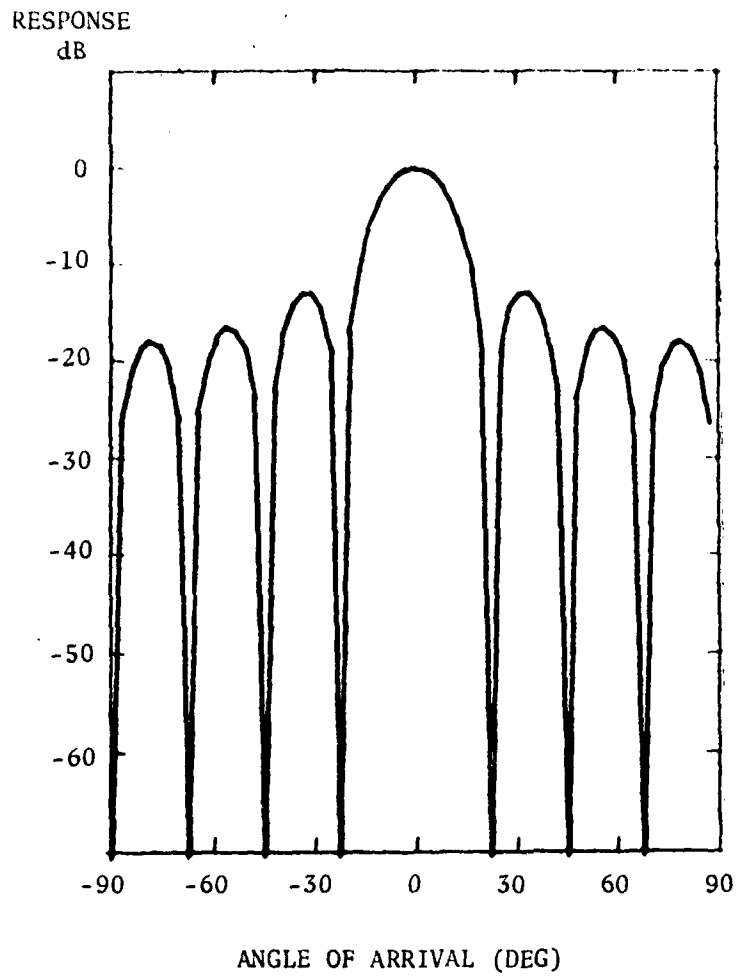


Fig. 3 Beampattern for uniform-weighted conventional array processor.  
 (Normalized to grating lobe spacing)

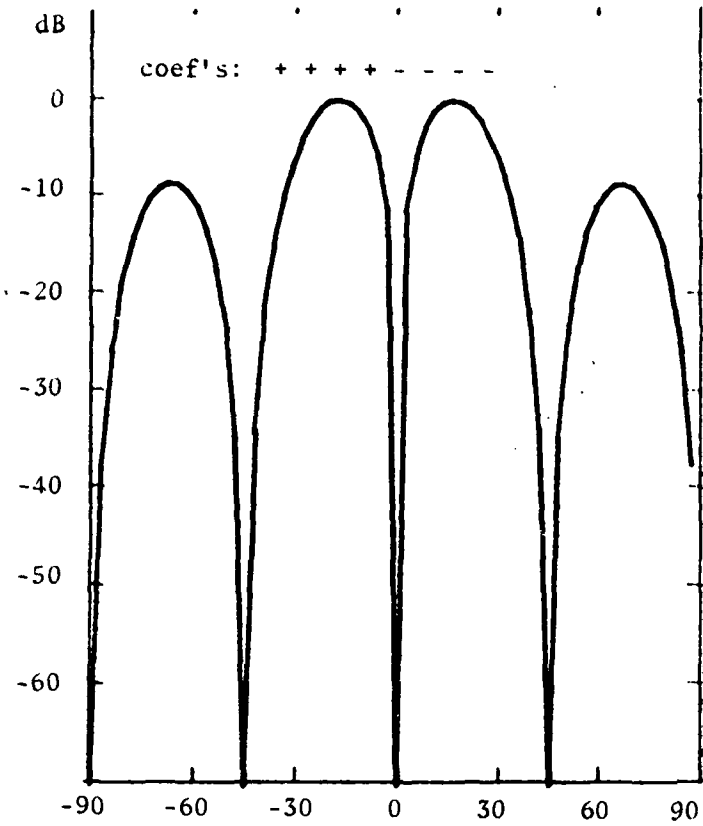


Fig. 4 a) Preprocessor pattern, Walsh #1.

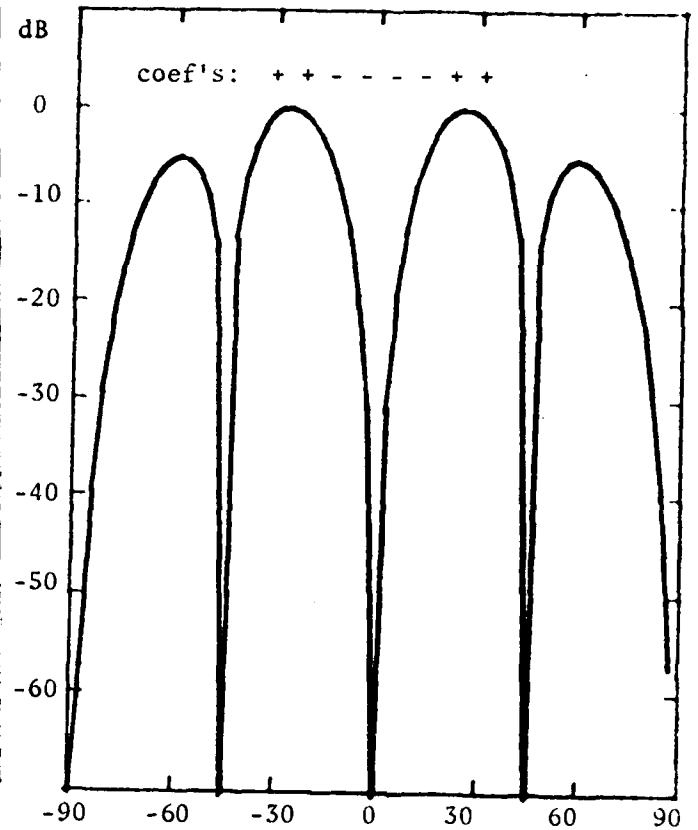


Fig. 4 b) Preprocessor pattern, Walsh #2.

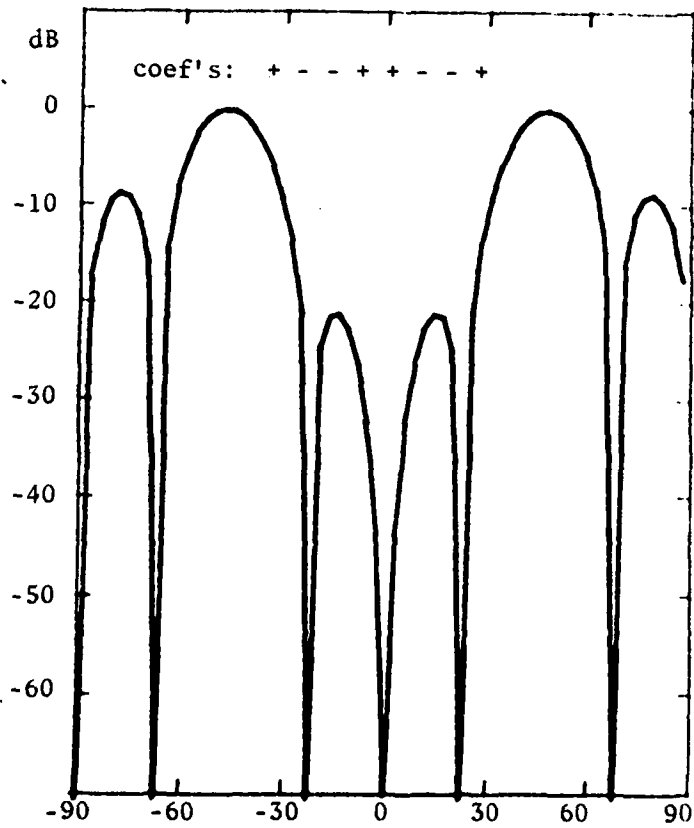


Fig. 4 c) Preprocessor pattern, Walsh #3.

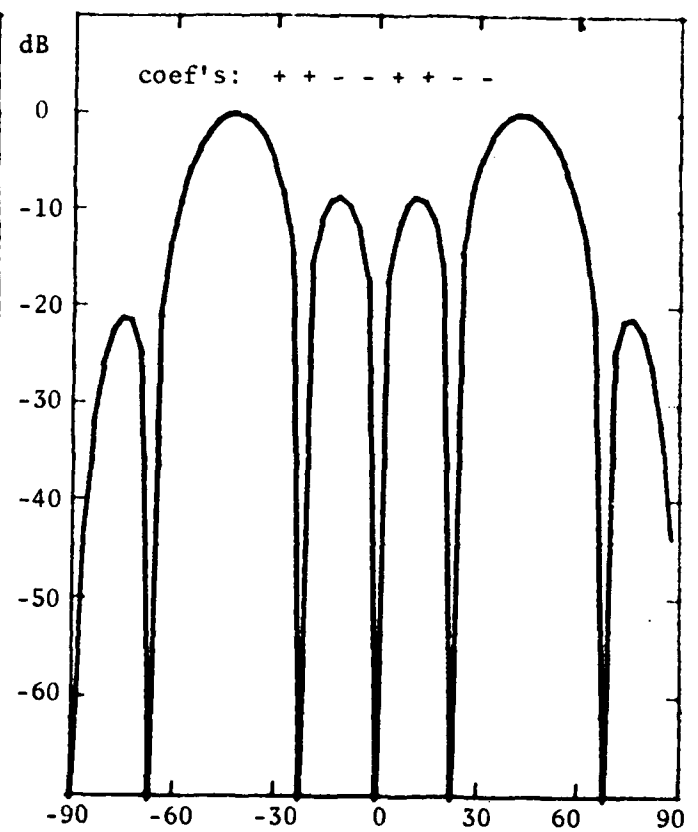


Fig. 4 d) Preprocessor pattern, Walsh #4.

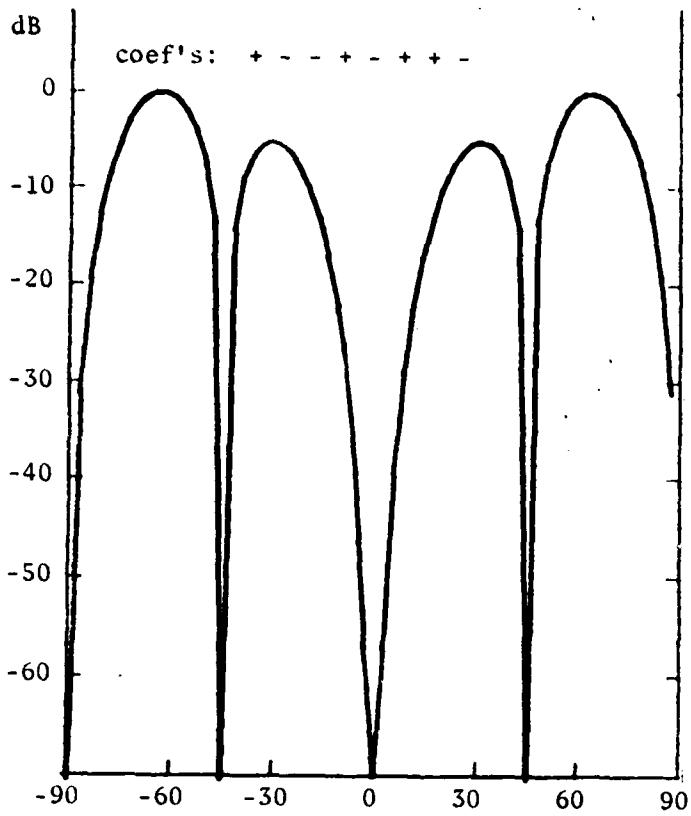


Fig. 4 e) Preprocessor pattern, Walsh #5.

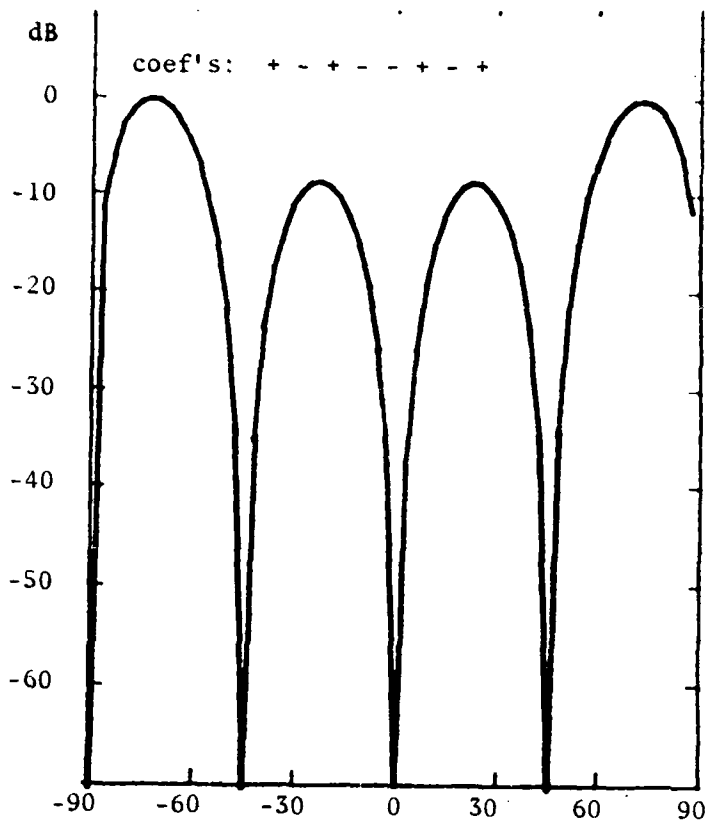


Fig. 4 f) Preprocessor pattern, Walsh #6.

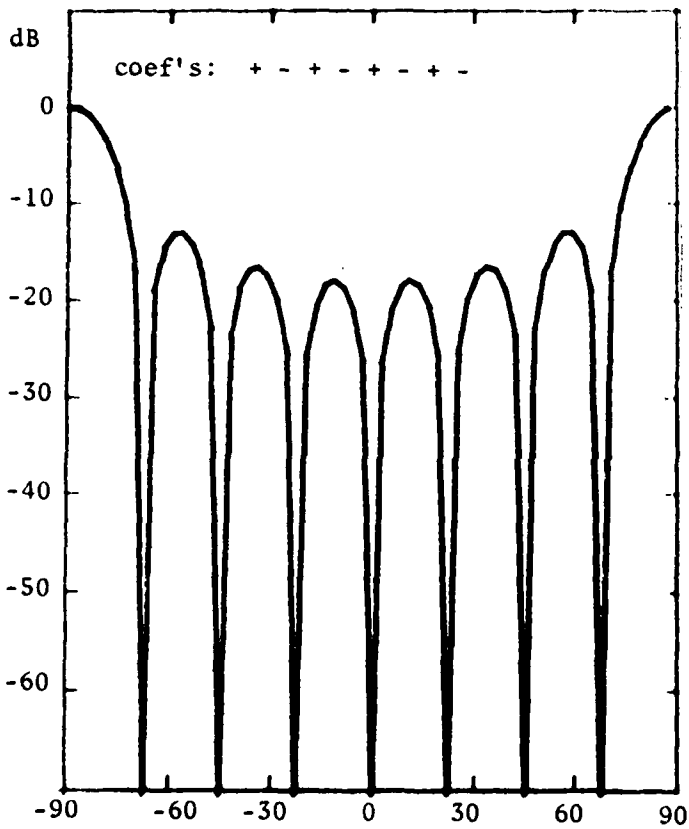


Fig. 4 g) Preprocessor pattern, Walsh #7.

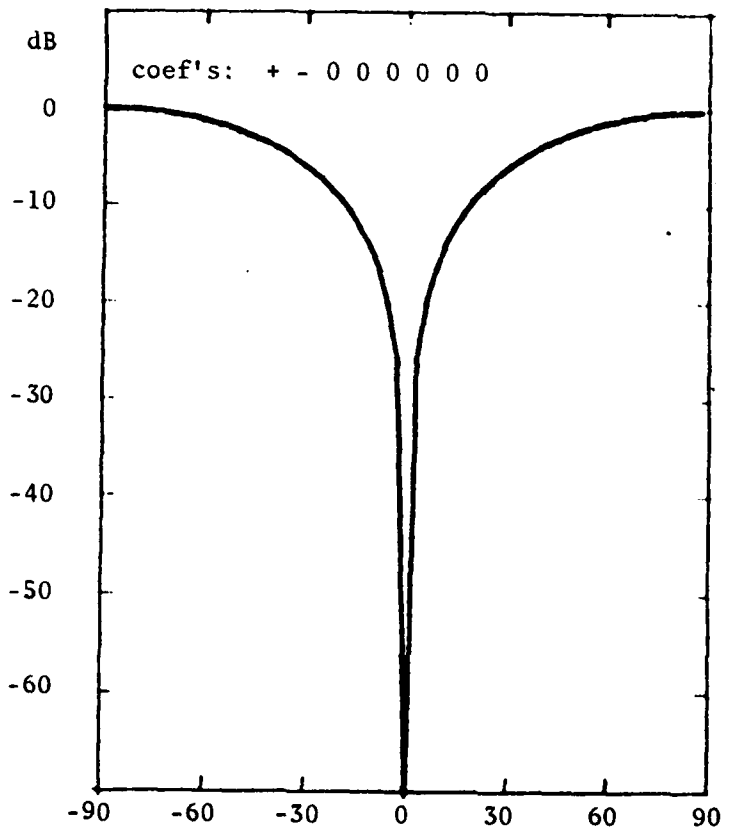


Fig. 5 Pattern for difference preprocessor.

Albuquerque, New Mexico and Los Lunas, New Mexico. The Albuquerque repeater was operated at -20 dB signal level and introduced a 23-Hz doppler frequency prior to retransmission. It was used to simulate a desired target signal. The interfering signal, produced at Los Lunas contained a 20-Hz doppler and was operated at -30 dB signal level. An azimuthal bearing difference of  $2.4^\circ$  is subtended between these transmitters when viewed from the receiving array in Los Banos, California.

A representative range-doppler map, as observed using a 1-sec dwell at the conventional beamformer output, is shown in Fig 6. The corresponding doppler spectrum is depicted in Fig. 7. A one-pulse MTI filter was employed at each subarray output, prior to beamforming. The upper trace and lower trace are the peak and RMS responses, respectively, over the 15 range gates.

Several displays of this type were examined during the course of the experimental study. Investigation revealed that the fourth subarray in the data set was producing an incorrectly beamformed output. It was later verified that this was due to a system hardware failure. For this reason, the results reported below for both convergence time constant studies and the optimum choice of initial weight vector were based on calculations in which the output from subarray number four was set to zero. In the element gain variation study, however, this failure proved to be useful in demonstrating the reduced sensitivity of an adaptive array to hardware failures. Details are presented in the sections following.

#### i) Convergence Time Constant Studies

In order to minimize the effects of adaptation start-up transients on the range/doppler map, it is desirable to have a time constant which is small

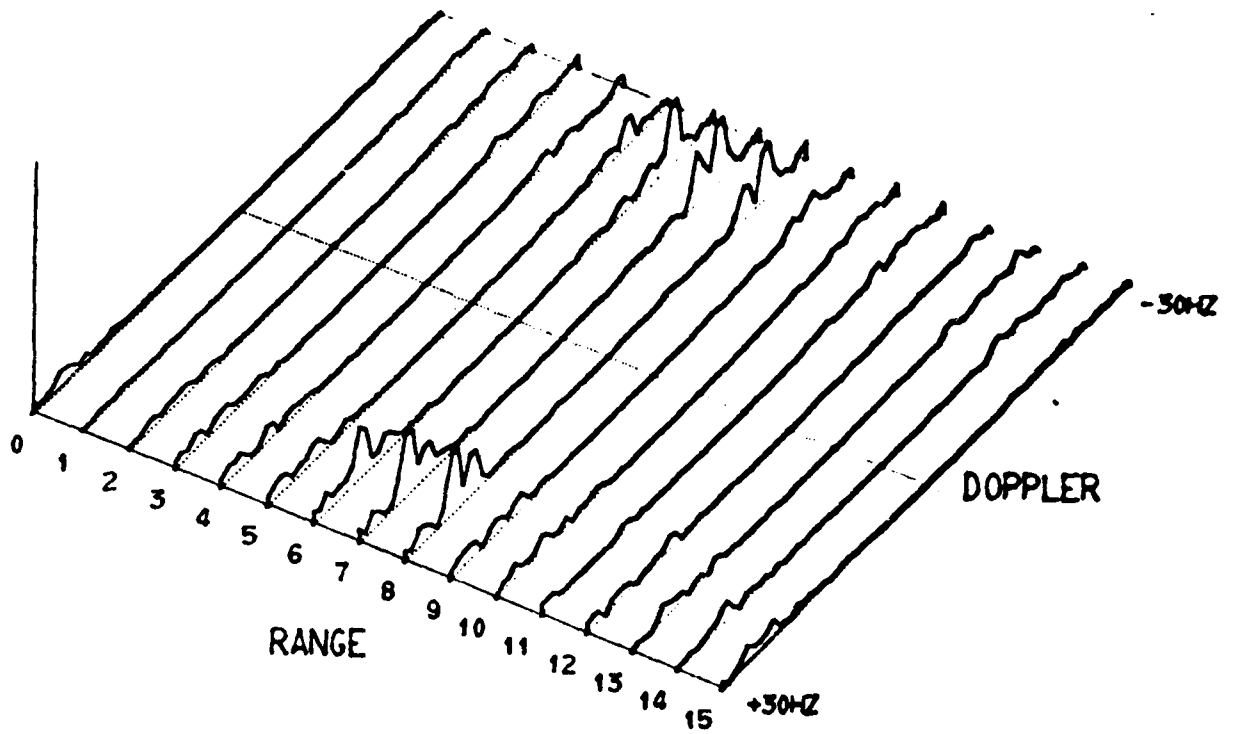


Fig. 6 Range—doppler map for 1-sec dwell from WARF tape RML 0030, File 64, using conventional beamformer.

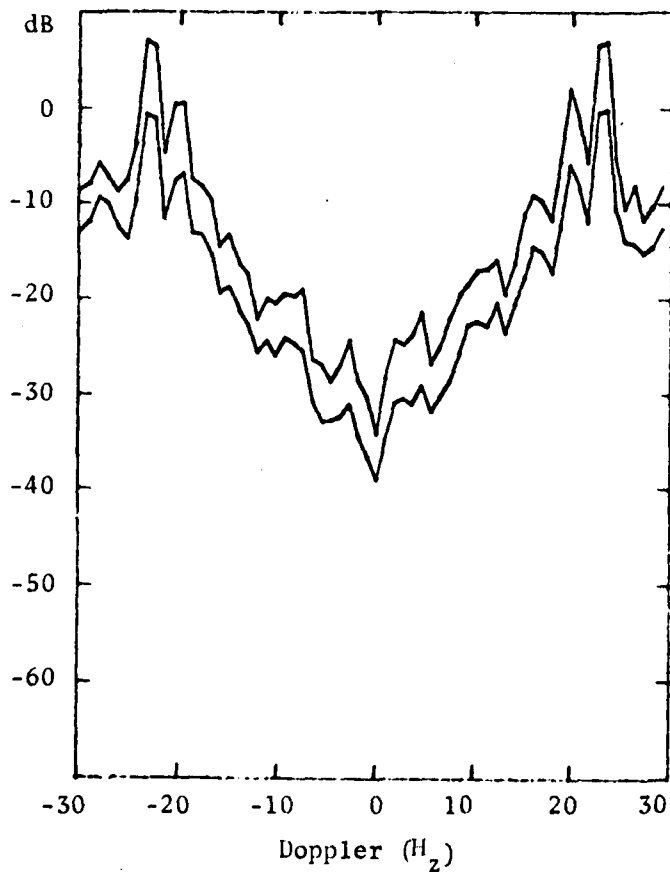


Fig. 7 Doppler spectrum using conventional beamformer.

compared with the radar dwell time. Two methods for reducing the adaptive time constant were investigated during the course of this study. The first involved the use of large adaptive step sizes and the second employed a modified adaptive algorithm based on the conjugate gradient method of Hestenes [12].

a) Increased Adaptive Step Size

The generalized sidelobe cancelling array structures introduced previously use the LMS algorithm to minimize the array output power. Thus, for both P-vector and linearly constrained beamforming, the weight update algorithm can be expressed (see Eqs. (23), (24), and (28)) as:

$$w(k+1) = w(k) + \mu \Delta(k) \quad (44)$$

where  $\Delta(k)$  is the product of the array output signal  $y_0(k)$  and the signal observed at weight  $w(k)$  at the  $k$ th adaptation. As shown by Widrow [8], the convergence rate of this algorithm is proportional to the step size parameter  $\mu$  with faster rates being achieved with larger  $\mu$  values. Using a normalized step size given by

$$\mu = \frac{\alpha}{\sigma_x^2 K L} \quad (45)$$

where  $\sigma_x^2 = E[x^2(k)]$ , it can be shown that the time constant of adaptation  $\tau_a$  is given approximately as

$$\tau_a \approx \frac{K L}{\alpha} \quad (46)$$

adaptations. Thus, an eight-element beamformer with four adaptive weights per delay line requires  $32/\alpha$  iterations to converge within  $1/e$  of the steady-state value. (It should be noted, however, that these results are valid only for  $\alpha$  in the range  $0 < \alpha < 1$ .)

To achieve rapid convergence, the above discussion suggests that  $\alpha = 1$  should be used. Unfortunately, values of  $\alpha$  near unity are impractical due to the resulting unacceptably large increase in output noise which is produced by the weight iteration. Widrow has termed this noise misadjustment and has shown that the fractional increase in output noise is given by  $\alpha$ . Thus, rapid adaptation is always accompanied by an increase in output noise and this noise level must be considered by the system designer when selecting the appropriate operating value for  $\alpha$ . Typical values which have been found to provide satisfactory performance using eight-element WARF data are in the range  $0.01 < \alpha < 0.1$ .

One additional property of adaptive arrays which incorporate large step sizes has also been observed. As discussed above, the system weights are updated by an amount proportional to the product of the array output signal and the signal present at the weight which is being updated. When the array signals contain large amplitude sinusoids at several frequencies, this product results in sum and difference frequency terms. Because the weights, in turn, multiply the data signals, a modulation of the incoming data may occur. Modulation at sum and difference frequencies has been observed in the processing of WARF data using values of  $\alpha$  which exceed 0.1.

Figure 8 shows the result of processing the RML 0030, file 64 data using  $\alpha = 0.16$  and four taps on each delay line. Linearly constrained beamforming was used with a difference (D) preprocessor. Comparison of Figs. 7 and 8 shows that adaptive processing has eliminated the interfering Los Lunas repeated at  $\pm 20$  Hz doppler, but numerous modulation products are evident in the display. These results indicate that the selection of optimal  $\alpha$  must be sufficiently small so as to eliminate the possibility of producing false targets in this manner. It should be noted that modulation products

are not observed at  $\alpha = 0.16$  when either clutter is present or when the input spectrum contains a multiplicity of waveforms and interference. Values of  $\alpha < 0.1$  have not been observed to produce these products in field-recorded data.

b) Conjugate Gradient Adaptation

An alternative approach to decreasing the time constant of an adaptive sidelobe cancelling array involves using a second-order weight update algorithm. (The LMS algorithm in (44) is first order in the weights in that  $w(k+1)$  depends only on  $w(k)$  and not on  $w(k-1)$ ,  $w(k-2)$ , etc.) One approach to higher-order adaptation is the conjugate gradient technique [9,12] which may be expressed as

$$w(k+1) = (1 + \beta) w(k) - \beta w(k-1) + \mu \Delta(k) \quad (47)$$

where  $0 \leq \beta < 1$ . It has been shown that this method produces faster convergence than does the first-order algorithm in (44) for the case of deterministic surface searching, provided that  $\beta$  is selected correctly. The optimum value for  $\beta$  is data dependent and is not a simple function of the data.

In order to examine this algorithm, the data shown in Figs. 7 and 8 were processed using several values for  $\beta$ , with  $\alpha$  fixed at 0.16. The processor parameters were identical to those used to compute the result shown in Fig. 7. In each case, a doppler spectrum was computed and four parameters were measured using this spectrum. The parameters were as follows:

SIL = Signal-to-interference ratio (dB) for signal at -23 Hz and interference at -20 Hz.

SPL = ratio of desired signal at -23 Hz doppler to spurious modulation component at -17 Hz.

SIR = Signal-to-interference ratio for desired signal at 23 Hz and interference at 20 Hz.

SPR = Signal to spurious ratio for desired signal at 23 Hz and modulation component at 17 Hz.

Table I summarizes the measured value of these parameters over the range of  $\beta$  values studied.

Table I  
Signal, interference, and spurious parameters  
for conjugate gradient algorithm  
( $\alpha = 0.16$ , 4 taps/element,  $W_S = D$ )

| <u><math>\beta</math></u> | <u>SIL</u> | <u>SPL</u> | <u>SIR</u> | <u>SPR</u> |
|---------------------------|------------|------------|------------|------------|
| 0                         | 16.1       | 8.1        | 14.9       | 13.3       |
| 0.1                       | 16.3       | 8.2        | 14.4       | 13.1       |
| 0.3                       | 16.8       | 8.4        | 13.3       | 12.6       |
| 0.5                       | 18.1       | 8.8        | 12.0       | 11.6       |
| 0.7                       | 15.9       | 9.6        | 10.8       | 9.5        |
| 0.9                       | 8.3        | 8.0        | 12.1       | 1.4        |

Based on these results, a best value of  $\beta = 0.5$  was selected. The doppler spectrum for this case is shown in Fig. 9. Note that  $\beta = 0$  corresponds to the first-order or LMS algorithm which produced the results given in Fig. 8. Comparison of these spectra shows that the second-order approach provides slightly greater rejection of the interferer at -20 Hz but at the cost of generally higher levels of modulation components. These products are also more numerous than in the first-order case.

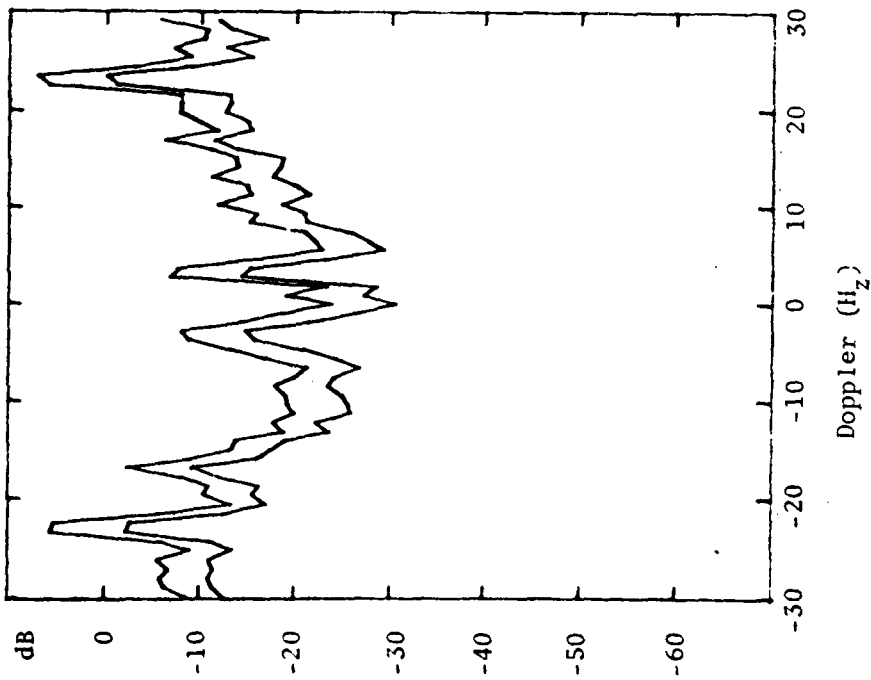


Fig. 8 Doppler spectrum using 1st order adaptive algorithm with no pre-adaptation,  $\alpha = 0.16$ .

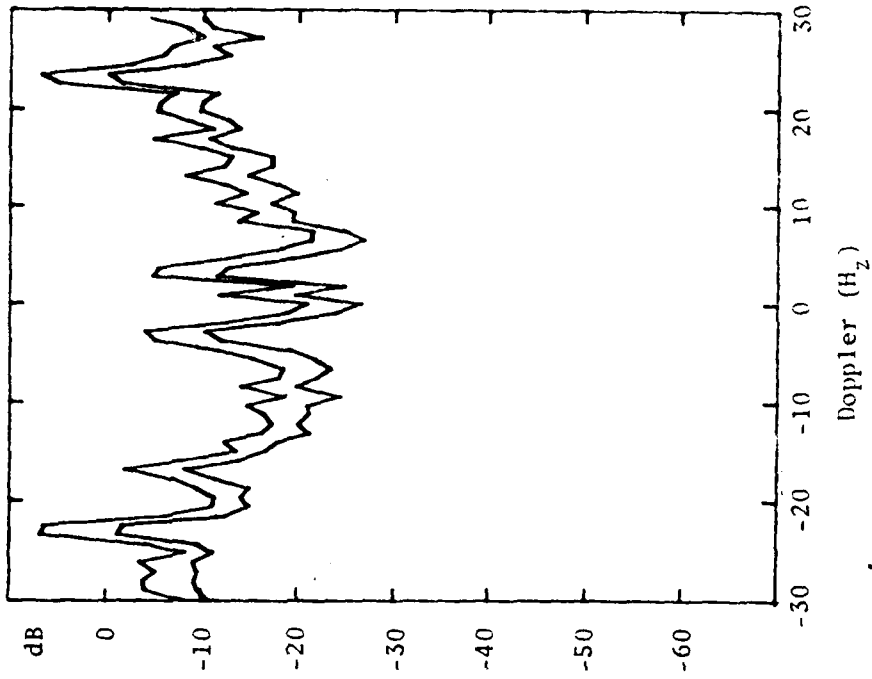


Fig. 9 Doppler spectrum using 2nd order adaptive algorithm with no pre-adaptation,  $\alpha = 0.16$ ,  $\beta = 0.5$ .

The effect of start-up time on algorithm performance was also investigated. A pre-dwell time increment of 0.125 sec was used to attempt to adapt out any initialization transients. This period was then followed by continuous adaptation during a 1-sec dwell. Figures 10 and 11 illustrate the doppler spectra obtained using the first- and second-order algorithms, respectively, in this manner. Comparison with Figs. 8 and 9 shows that the initialization adaptation offers no measurable advantage.

It is very important, however to maintain adaptation through the dwell interval. Evidence of this fact is presented in Figs. 12 and 13 which were obtained by adapting only during the 0.125 sec pre-dwell time period. The system weights were then fixed during the ensuing 1-sec dwell interval. Although no spurious signals can be seen (due to the fact that constant weight values were employed), interference rejection is approximately comparable with the conventionally processed spectrum presented in Fig. 7. Table II summarizes the parameter values measured from the spectra in Figs. 7-15.

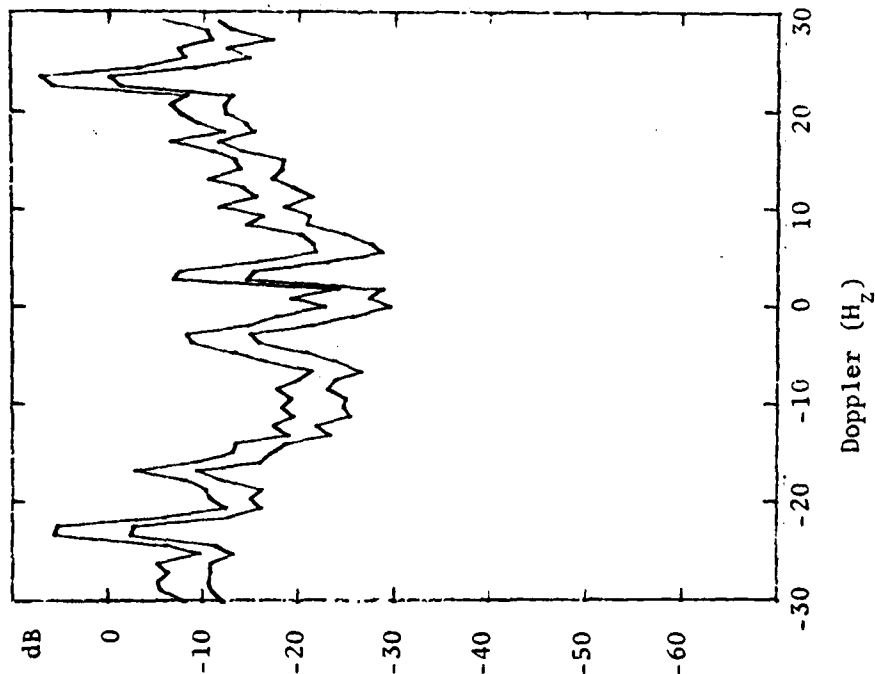


Fig. 10 Doppler spectrum using 1st order adaptive algorithm with pre-adaptation,  $\alpha = 0.16$ .

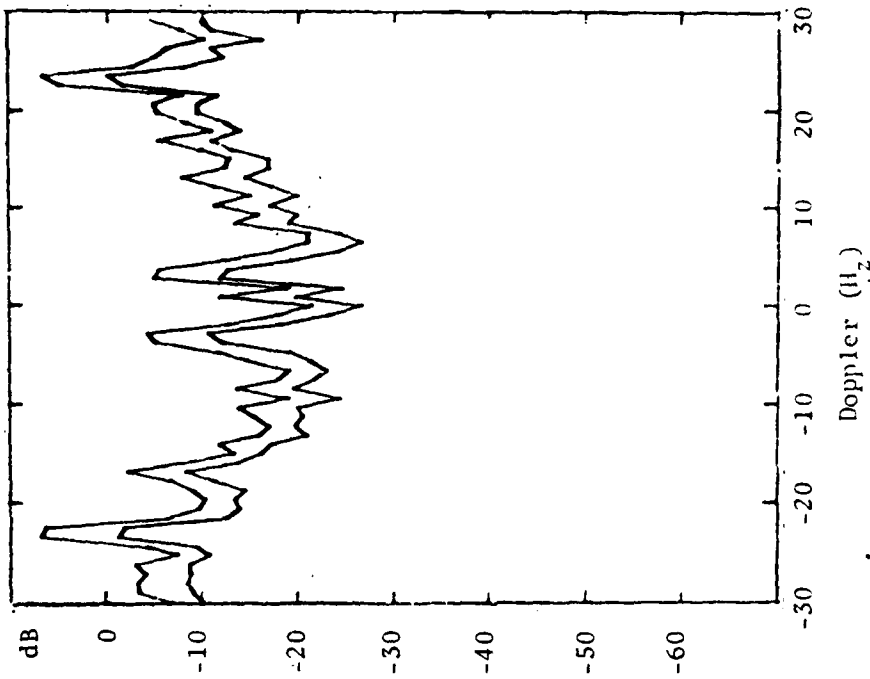


Fig. 11 Doppler spectrum using 2nd order adaptive algorithm with pre-adaptation,  $\alpha = 0.16$ ,  $\beta = 0.5$ .

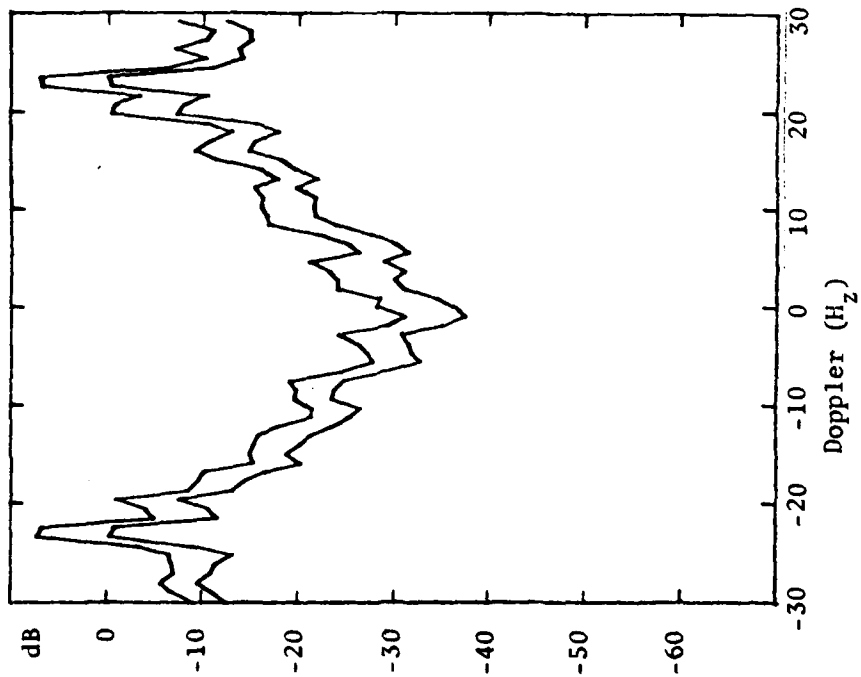


Fig. 12 Doppler spectrum using 1st order adaptive algorithm only during pre-adaptation period,  $\alpha = 0.16$ .

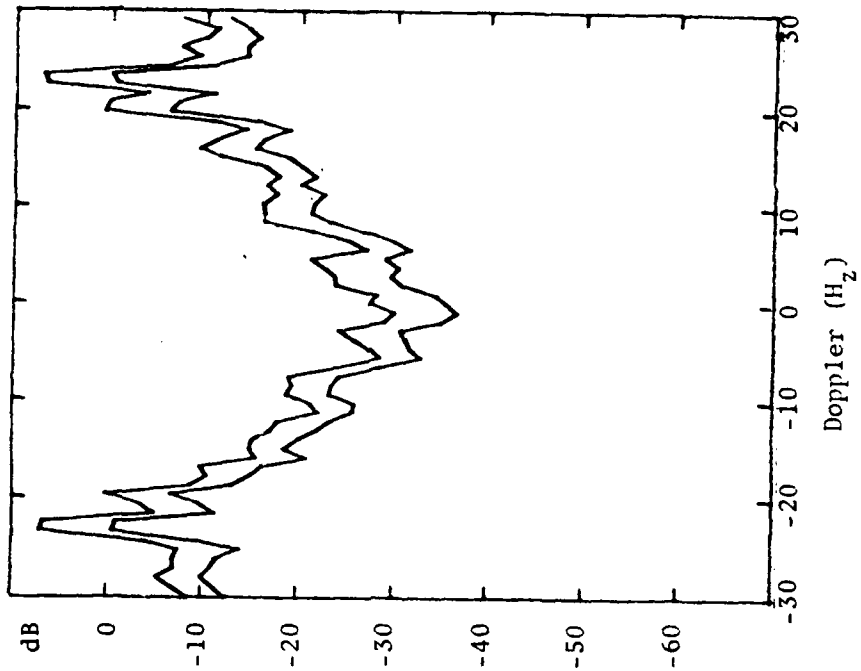


Fig. 13 Doppler spectrum using 2nd order adaptive algorithm only during pre-adaptation period,  $\alpha = 0.16$ ,  $\beta = 0.5$ .

Table II  
Signal, interference, and spurious parameters  
for doppler spectra shown in Figs. 7-13

| PROCESSING  | SIL  | SPL      | SIR  | SPR      |
|---|------|----------|------|----------|
| Conventional (Fig. 7)                                       | 6.6  | $\infty$ | 4.8  | $\infty$ |
| 1st order during pre-dwell,<br>fixed during dwell (Fig. 12) | 8.3  | $\infty$ | 7.5  | $\infty$ |
| 2nd order during pre-dwell,<br>fixed during dwell (Fig. 13) | 7.1  | $\infty$ | 6.4  | $\infty$ |
| 1st order, no pre-dwell<br>(Fig. 8)                         | 16.1 | 8.1      | 14.9 | 13.3     |
| 2nd order, no pre-dwell<br>(Fig. 9)                         | 18.1 | 8.8      | 12.0 | 11.6     |
| 1st order, with pre-dwell<br>(Fig. 10)                      | 16.3 | 8.4      | 14.8 | 13.6     |
| 2nd order, with pre-dwell<br>(Fig. 11)                      | 17.2 | 9.1      | 11.8 | 12.0     |

ii) Array Element Gain Variation Studies

The undesirable effects of array element gain variation on the performance of an adaptive array is readily apparent in the sidelobe cancelling decomposition shown in Fig. 2. The spatial preprocessor  $W_S$  is designed to block the desired signal from the lower, or noise cancelling, path. As discussed previously, this design is based on the fact that the desired signal is modelled as being in phase and having identical amplitudes at the array element outputs--see Eq (2). If this is not the case, a desired signal component will appear at the  $W_S$  outputs and after filtering by the tapped-delay-lines,

this component will be subtracted from the desired signal component which is present in the upper conventional path. The net result is generally a combination of signal amplitude reduction and distortion.

Widrow, et al. [13] have termed this problem "signal leakthrough" and have presented a discussion of its effects on adaptive noise cancelling. Since cancellation is based on a reduction of total output power, signal leakthrough becomes significant only if the desired signal power in the tapped-delay-lines shown in Fig. 2 becomes comparable with the levels of noise and interference in those lines. In effect, the degrees of freedom represented by the tap weights are used to cancel interference rather than desired signal if the latter is of sufficiently low amplitude. As a specific example, it has been shown [13] that if the SNR out of  $W_S$  is -10 dB, then the signal distortion at the cancelled output will be less than 5%. In the HF applications of interest in this report, the element SNR's are generally -10 dB or less and the spatial nulling beams in the prefilters shown in Figs. 4 and 5 should provide at least 10 dB of additional desired signal rejection.

Thus, it is not anticipated that signal leakthrough will present a significant problem in HF adaptive arrays under normal operating conditions. One potential area of concern, however, is that of element component failure. For example, if the amplifier on one of the array elements fails, and a difference preprocessor is used, no signal rejection will be applied to the two  $W_S$  outputs which are derived from that element. Another similar failure mechanism would be that of misdirecting the subarray steering due to hardware failure. This would have the effect of producing a significant gain and phase error at that subarray output.

Either of the above failure mechanisms could produce significant signal leakthrough problems at high element SNR--e.g., 0 dB --such as those found in the data recorded on July 10, 1975 at WARF. As discussed previously, subarray element number four did contain a beamforming error during this time period. The effect of this failure, as well as simulated failures in other subarrays was studied to determine the sensitivity of both conventional and adaptive beamforming methods. Both the difference (D) and Walsh (W) preprocessor structures were investigated, and both P-vectors and linearly constrained algorithms were employed.

The results obtained using the difference processor on the dwell which produced the doppler spectrum shown in Fig. 7 are summarized in Fig. 14. This plot illustrates the signal-to-interference level at -23 Hz and -20 Hz (SIL) obtained for conventional (C), P-vector difference adaptive (PD), and linearly-constrained difference adaptive (CD) processing. The abscissa indicates the subarray channels which were set to zero prior to processing in order to simulate the effect of subarray failures. Thus, the extreme left-hand points represent processing the data as originally recorded, the point labelled 4 indicates that the output from subarray 4 was set to zero prior to processing, and 4,5,6 shows that three of the eight outputs were zeroed.

Note that eliminating element four improves performance for all three processors. This is due to the beamforming error known to be present in the data from subarray four. The results indicate that conventional processing is considerably more affected by element failure than is adaptive processing, particularly when subarray 1 is dropped. In general, the constrained processor appears to offer a slight advantage over the P-vector processor

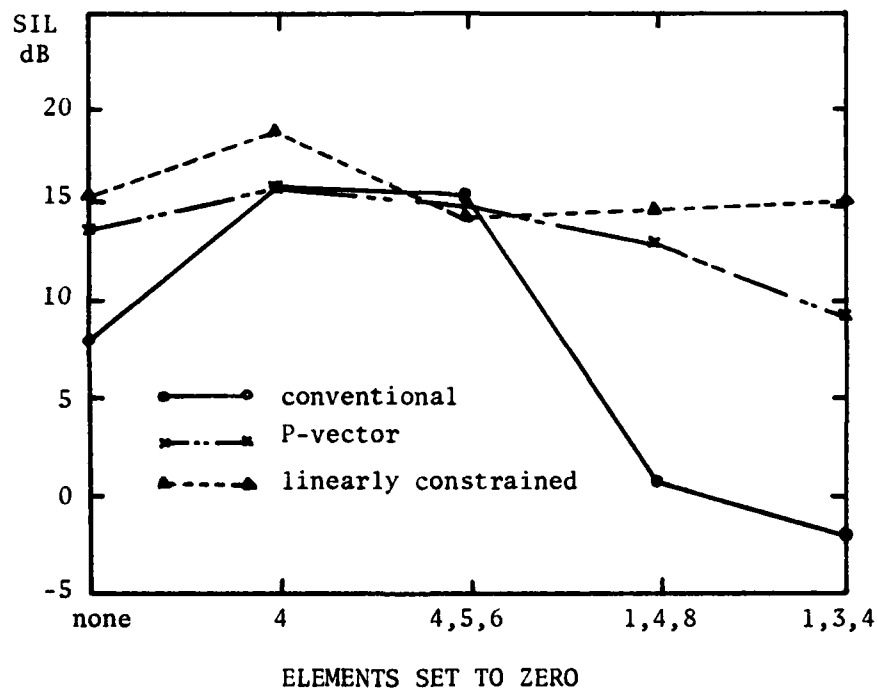


Fig. 14. Signal-to-interference ratios observed as a function of array geometry using difference preprocessor.

for this particular dwell. The range-doppler spectra for the 1,3,4 failure case are particularly interesting and are presented in Fig. 15.

Similar results were obtained when the Walsh preprocessor was used on the same data. Figure 16 shows the SIL values for the same dwell and element failures illustrated in Fig. 14. The only significant difference between Figs. 14 and 16 is that the Walsh preprocessor results in 1-2 dB poorer adaptively processed SILs than does the difference preprocessor.

### iii) Optimum Choice of Initial Weight Vector

The final topic addressed in this report is that of choosing the best set of tapped-delay-line coefficients to be used at the beginning of each dwell. Clearly, the transient effects of adaptation are minimized when this initial set is close to the final steady-state adapted coefficients. To assess these effects, three different methods of choosing the initial weights were investigated:

- a) An adaptive "start-up" period was employed by adapting on data immediately prior to the dwell of interest.
- b) The coefficients were set to zero at the beginning of each dwell.
- c) The coefficients were set to values equal to those obtained at the end of the last radar dwell having the same steering direction and operating frequency as the current dwell.

A variety of radar data was processed and the doppler spectra obtained with these three methods were compared. It was found that the first two produced virtually identical results and that method c) was inferior by less

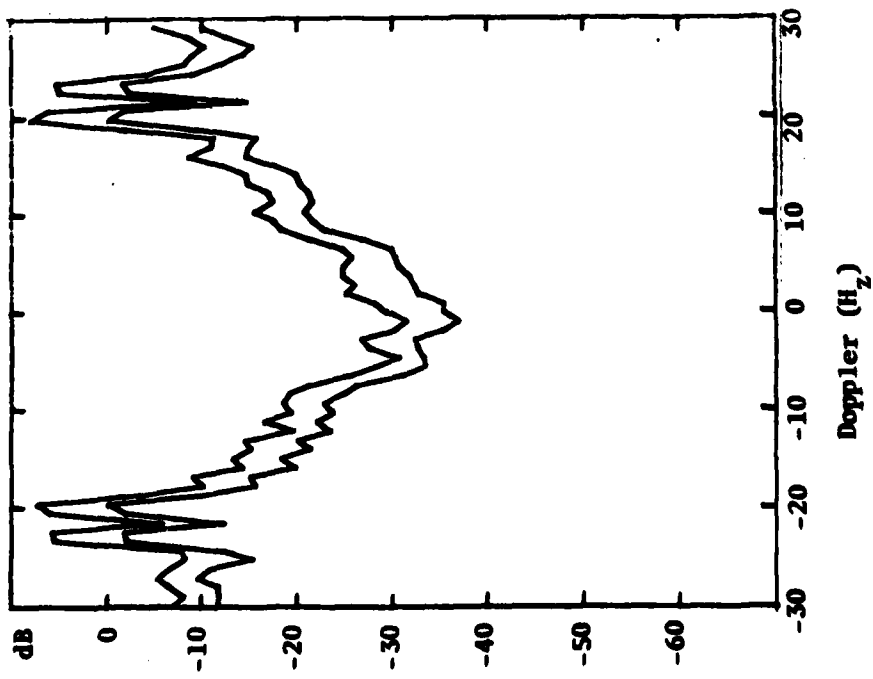


Fig. 15 a) Doppler spectrum using conventional beamforming with elements 1,3,4 set to zero.

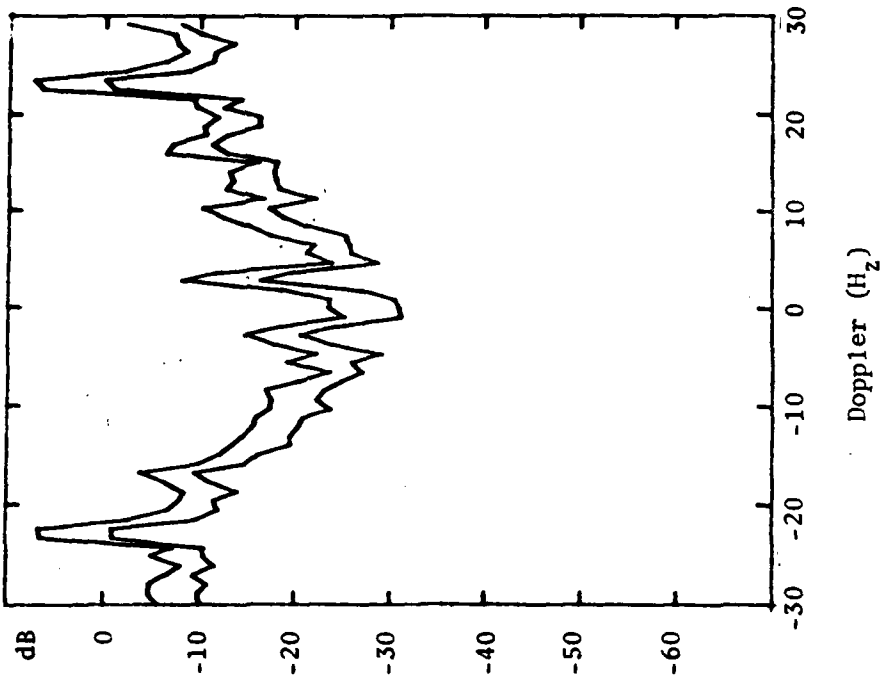


Fig. 15 b) Doppler spectrum using linearly constrained adaptive beamformer with elements 1,3,4 set to zero.

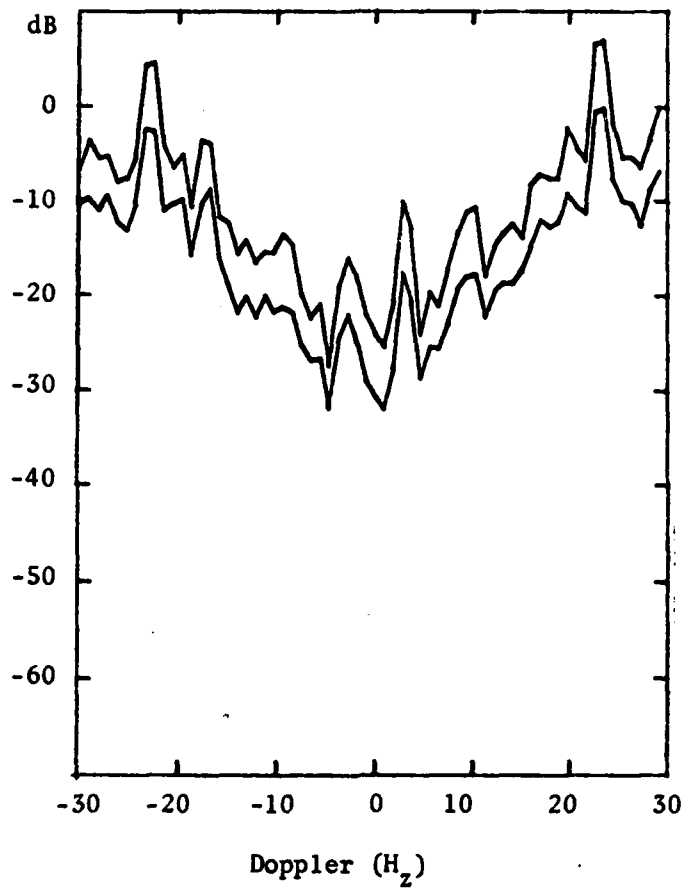


Fig. 15 c) Doppler spectrum using P-vector adaptive beamformer with elements 1,3,4 set to zero.

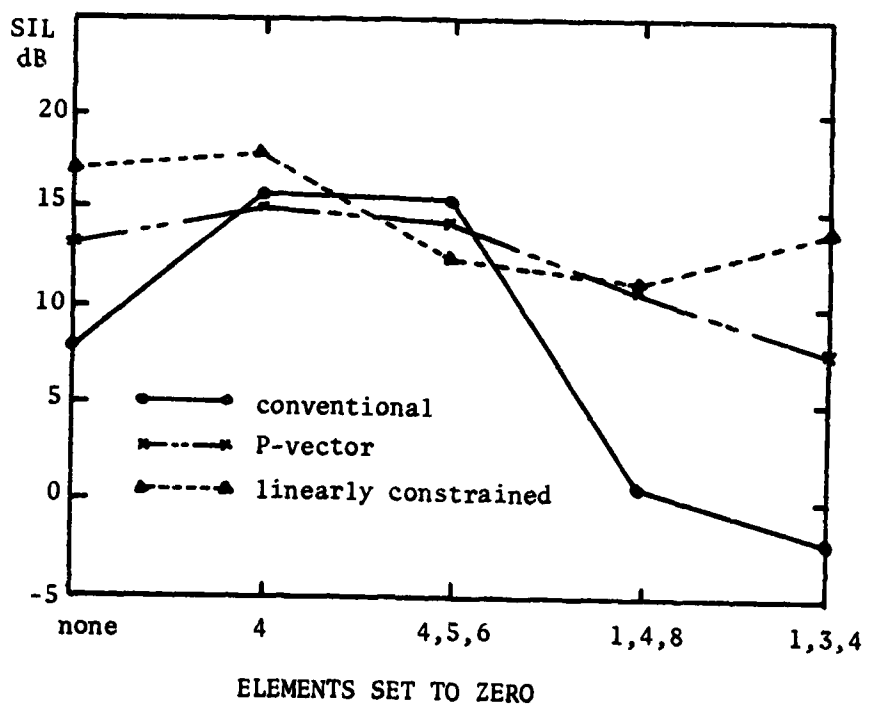


Fig. 16 Signal-to-interference ratios observed as a function of array geometry using Walsh preprocessor.

than 1 dB on some dwells. This minor difference is attributed to the inherent time-varying nature of HF data, as illustrated in Figs. 7-11 above. Since method b) is the easiest to implement, it is the recommended approach.

#### IV DISCUSSION AND CONCLUSIONS

This report has introduced a new formulation for adaptive arrays, termed generalized sidelobe cancelling. It was shown that this formulation is both an alternative method of implementing previous adaptive structures as well as a method which can be used to formulate a new, wider class of adaptive beamformers. The GSC approach also provides an implementation advantage, in that the conventional beamformer is separated out as a distinct element in the overall processor. In addition, the linear constraints which ensure no distortion in the main lobe can be implemented as simple analog hardware elements. This is in contrast to previous approaches in which the constraints have been incorporated into the adaptive algorithm. A fourth advantage of the GSC formulation is that it clearly delineates the similarities and differences between P-vector and linearly constrained adaptive beamforming.

The GSC beamformer was used to study field-recorded WARF data in order to further assess the performance characteristics of adaptive processing of HF radar data. As a result of these studies, we conclude the following.

1. Effective interference rejection can be achieved by adapting within the radar dwell with initial weight values set to zero. Preadapting, or warm-up periods, are not required. This is equivalent to initializing the overall processor to a conventional beamformer.

2. Second-order accelerated-convergence algorithms have not been shown to provide significantly improved radar performance. These algorithms require the specification of an additional adaptive parameter and the difficulties of choosing the best value for this parameter offset any advantages offered by the algorithms.

3. The simple difference preprocessor  $W_S$  is at least as effective as the orthogonal Walsh preprocessor and was shown to be 2 to 3 dB better in some cases. This is somewhat surprising in that it has been shown that the two methods have exactly the same steady-state performance in a stationary environment. Any differences are therefore attributable to the time-varying nature of the HF data.

4. Adaptive array beamforming is less affected by major failures of array elements than is conventional beamforming. Loss of three of the eight subarrays was shown to induce a loss in performance of 10 dB for conventional processing and less than 4 dB for adaptive beamforming.

Because these conclusions are based on observation of an extremely limited data set, they may not be representative of those obtained as a result of extensive analysis. It is, however, significant that the existing form of the adaptive beamformer has been shown to be extremely robust over the range of data studied thus far. Changes in performance of a few dB have been noted, but interference rejection of the adaptive beamformer has consistently been significantly better than that provided by conventional beamforming.

Future work with the GSC processor should involve examination of larger data bases as well as additional theoretical studies. Possibilities in the latter case involve including both gain and phase filtering in the  $W_S$  preprocessor, studying alternative upper-loop algorithms in the P-vector formulation, investigating the use of the lattice-adaptive filter [14] in the GSC processor, and a study of the effects of quantization on overall performance of the adaptive beamformer.

## References

1. L. J. Griffiths and M. Larimore, "Adaptive array processing of HF signals propagated over a 2600 km path", RADC-TR-73-75, Final Technical Report, Rome Air Development Center, Griffiss AFB, New York, January, 1973.
2. L. J. Griffiths, "Adaptive array processing of HF backscatter radar signals", RADC-TR-74-194, Final Technical Report, Rome Air Development Center, Griffiss AFB, New York, May, 1974.
3. L. J. Griffiths, "Characteristics of adaptive beamforming methods in an HF backscatter environment", RADC-TR-75-205, Final Technical Report, Rome Air Development Center, Griffiss AFB, New York, August, 1975.
4. L. J. Griffiths, "Time-domain adaptive beamforming of HF backscatter radar signals", IEEE Trans. Antennas and Propagation, vol. AP-24, September, 1976.
5. L. J. Griffiths, "A comparison of quadrature and single-channel receiver processing in adaptive beamforming", IEEE Trans. Antennas and Propagation, vol. AP-25, March, 1977.
6. L. J. Griffiths, "Experimental results obtained using real-time, continuously-adaptive beamforming methods in an HF backscatter chirp radar system", NATO ASI on Signal Processing, Portovenere, Italy, August, 1976.
7. L. J. Griffiths, "An adaptive noise-cancelling procedure for multidimensional systems", Proc. Asilomar Circuits and Systems Conference, Asilomar, Calif., November, 1976.
8. B. Widrow, "Adaptive filters", in Aspects of Network and System Theory, R. Kalman and N. DeClaris, Eds., Holt, Rinehart, and Winston, New York, 1971.
9. G. R. Walsh, Methods of Optimization, Wiley, New York, 1975.

10. B. Widrow, et al., "Stationary and non-stationary learning characteristics of the LMS adaptive filter", Proc IEEE, August, 1976.
11. C. W. Jim and L. J. Griffiths, "Random gain and phase error effects in optimal array structures", TR EE 77-2, Dept. of Elec. Eng., Univ. of Colorado, Boulder, September, 1977.
12. M. Hestenes and E. Stiefel, "Method of conjugate gradients for solving linear systems", Report 1659, National Bureau of Standards, 1952.
13. B. Widrow, et al., "Adaptive noise cancelling: Principles and applications", Proc. IEEE, vol. 63, No. 12, December, 1975.
14. L. Griffiths, "An adaptive lattice structure for noise-cancelling applications", Proc. ICASSP, Tulsa, Oklahoma, April, 1978.